ACS Photonics

Article

pubs.acs.org/journal/apchd5

Selective Functionalization of the Nanogap of a Plasmonic Dimer

Xuan Zhou,[†,‡] Claire Deeb,[†,§] Sergei Kostcheev,[†] Gary P. Wiederrecht,[∥] Pierre-Michel Adam,[†] Jérémie Béal,[†] Jérôme Plain,[†] David J. Gosztola,[∥] Johan Grand,[⊥] Nordin Félidj,[⊥] Huan Wang,[†,¶] Alexandre Vial,[†] and Renaud Bachelot*[,†]

[†]Laboratoire de Nanotechnologie et d'Instrumentation Optique, CNRS UMR 6281, Université de Technologie de Troyes, 12 Rue Marie Curie CS42060, 10004 Troyes Cedex, France

[∥]Center for Nanoscale Materials, Argonne National Laboratory, Argonne, Illinois 60439, United States

[⊥]Interfaces, Traitements, Organisation et Dynamique des Systèmes, Université Paris Diderot, Sorbonne Paris Cité, CNRS UMR 7086, 15 rue Jean de Baïf, 75205 Paris Cedex 13, France

S *Supporting Information*

ABSTRACT: We report a self-developing anisotropic gold/polymer hybrid nanosystem that precisely places dye molecules at the plasmonic hotspot of metal nanostructures for sensing and photonics applications. Unlike conventional molecule−particle configurations, the anisotropic hybrid nanosystem (AHN) introduces an anisotropic spatial distribution of dye-containing active medium. This allows us to precisely overlap the near-field spatial distribution with the active medium and rule out the contribution from the background molecules. This overlap effect selectively highlights the optical response of the molecules of interest, that is, molecules located at the hotspots. Our AHN consists of gold nanodimers whose gaps have been filled with methylene blue molecules. They have been studied by plasmon-enhanced Raman spectroscopy as a probing tool. The AHN opens new doors not only for fundamental studies and photonics applications of molecule−particle interactions, but also for molecular trapping methods at the nanoscale.

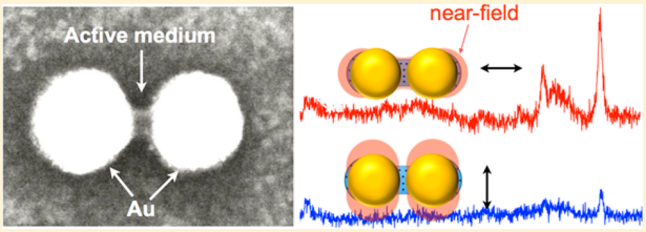

KEYWORDS: *photopolymerization, photonics, hybrid nanostructures, surface plasmons, surface-enhanced Raman spectroscopy*

Molecular plasmonics associated with molecule−particle interactions have become a very popular topic for plasmonics research because of the energy transfer between the two components.[1−3] This energy transfer has led to numerous promising applications of molecule/particle hybrids, such as nanoemitter,[4,5] photovoltaic,[6,7] sensing and optical imaging,[8−11] cancer therapy,[12,13] and plasmon-enhanced spectroscopies.[14,15] In these studies, the shape, size, and composition of metal nanoparticles are some key factors to vary, in order to achieve a plasmon field optimized in intensity or tunability.[16−19] Additionally, the molecule−particle distance[3,20] and chemical environment[21,22] play a significant role in plasmon-enhanced light emission. Although these factors have attracted great attention, a reasonable approach to selectively position molecules within the optical distribution of the electromagnetic field of plasmonic particles would have great impact. This would be highly advantageous for fundamental research and photonics applications.

Current approaches toward this goal include optical tweezers, which are well-known for placing a molecule or nanoparticle at a desired location.[23−25] This method allows for optical trapping of a single molecule or particle with a considerable trap confinement and high efficiency, but requires a liquid environment for any additional measurements on the trapped molecule/particle and continuous laser irradiation unless operating in vacuum. Chemical self-assembly with DNA molecules have been used as well to bring nano-objects to the particle vicinity.[26,27] This technique works well to obtain a random layer of nano-objects on the particle surface. However, the nano-object distribution does not allow for selectively targeting plasmonic hotspots. Alternatively, accurate nanoparticle positioning at plasmonic hotspots has been achieved by using light-assisted molecular immobilization.[28] Nevertheless, molecule delivery has not yet been reported.

In this article, we report on a convenient and effective approach to position dyes at plasmonic hot spots based on a self-developing plasmonic anisotropic hybrid nanosystem (AHN). We use surface-enhanced Raman scattering (SERS) to highlight the fact that there is considerable signal contribution of molecules that are not adsorbed on the nanoparticle surface, which has long been ignored by classical SERS.[29−32] The AHN is essentially a metal/dye-doped-polymer hybrid nanostructure with dye molecules spatially selectively placed via surface plasmon-triggered nanophotopolymerization.[33,34] AHNs in this article are constructed on the basis of either dimers or monomers of gold nanodisks. In the case of dimers, the varying gap size leads

Received: September 8, 2014
Published: December 9, 2014

to different near-field distributions and thus results in controllably distinct spatial distributions of dye molecules. Additionally, classical SERS with random dye molecule distributions on similar nanostructures are performed. The SERS signal contributions from the trapped molecules are highlighted through careful comparison between the two experiments. The use of isolated gold nanodisks as controls for the dimers reveals that even the hybrid nanosystem based on a simple symmetric nanostructure provides some optical anisotropy. This optical anisotropy introduces an extra-enhancement caused by the selective molecular distribution as well as its overlap with the dipolar optical near-field. In this article, a series of polarization-dependent SERS studies have been carried out on single nanohybrid particles for quantifying optical performance. Let us point out that the AHN has numerous potential applications, among which SERS is presented here as an example. For future applications of this nanohybrid, the active medium can be doped with quantum dots for polarization-controlled light-emitting systems with high photostability, or conductive molecules can be embedded within the polymer to be used for building a bridge between two coupled metal nanostructures, and so on.

Molecule Positioning. The gold nanodimers were fabricated following the top-down method based on electron-beam lithography (EBL) on an indium–tin oxide (ITO)-coated glass substrate. Each of the nanodisks was h = 50 nm in height and R = 35 nm in radius. The particle separation between the two nanodisks was designed to vary from g = 0 to 50 nm in a step of 5 nm. Methylene blue (MB), the target molecule for this SERS study, can be trapped by photopolymer nanostructures through nanoscale photopolymerization, a process that imprints the near-field of the metal nanostructures.[33,34] MB (0.50 wt %) actually serves as both a SERS molecular probe and photosensitizer (in the red part of the spectrum) in the polymerizable formulation, and is mixed with two other components 95.52 wt % pentaerythritol triacrylate (PETIA) and 3.98 wt % methyldiethanolamine (MDEA). Figure 1a shows the absorption spectrum of MB dissolved in PETIA. The photopolymerizable solution is characterized by a threshold dose (D_{th}) that describes the lowest energy required for inducing photopolymerization.[35] A λ_0 = 647 nm laser with an incident dose $D_0 = 65\%D_{th}$ was used so that the incident field could not initiate any photopolymerization. During laser irradiation, the plasmonic field supported by the metal nanostructure enhances the local electromagnetic field intensity above the threshold to produce a polymer. More details about the nanophotopolymerization have been stated in our previous studies.[33,34,36−39] By aligning the incident polarization along the interparticle axis of the dimer (X-axis), MB molecules can be "frozen" in polymer structures that are fabricated along the long axis of the nanodimer, most likely in the gap. The photopolymerization is followed by a rinsing process with ethanol and isopropanol to clean the unpolymerized dye-containing solution, leaving only molecules in the polymer nanostructures for SERS studies (see Figure 1b). Figure 1c is the image of a typical hybrid nanostructure characterized by scanning electron microscopy (SEM). The secondary electron detector of the SEM provides different contrasts for metal and the MB-containing photopolymer nanostructures. Based on this obtained metal/dye-doped-polymer hybrid nanostructure that controls the spatial positions of molecules, we studied the SERS response from single nanostructures with a confocal Raman spectrometer under an excitation wavelength of λ_{exc} = 633 nm. The excitation and detection region was 1 μm in diameter. Different polarizations were used for studying the effect of overlapping the plasmonic field with the MB molecules in the gap of the dimers.

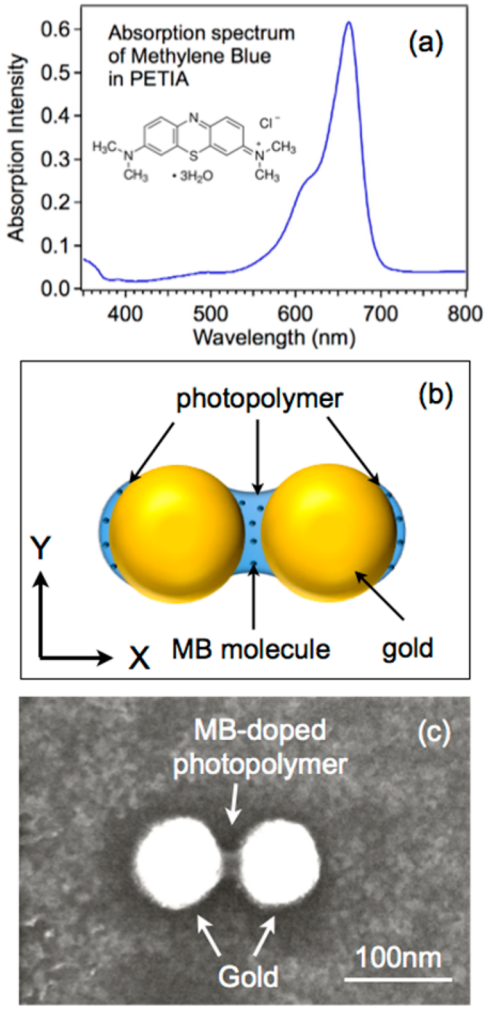

Figure 1. (a) Absorption spectrum of methylene blue molecules dissolved in the monomer PETIA. The chemical structure of MB is shown in the inset. (b) Scheme of a hybrid nanodisk with MB molecules selectively positioned at the plasmonic hotspots. (c) SEM image of a hybrid nanodimer. The metal and the photopolymer are distinguished by different contrasts.

RESULTS AND DISCUSSION

Topographic Characterization. For a given gold nanodimer, both initial (before polymerization) and hybrid nanostructures (after polymerization) were characterized by AFM for more topographic information. The differential AFM image, namely, the result of a pixel-by-pixel image calculation of the AFM image obtained *before* polymerization subtracted from the AFM image taken *after* polymerization on the same nanoparticle, was obtained for highlighting the integrated MB-containing polymer nanostructures. Figure 2a and b illustrate the differential AFM images of two typical dimers with gap sizes of 25 and 45 nm, respectively. Figure 2c and d are the corresponding cross-section profiles that display the position of the integrated polymer by peaks of polymer height, obtained by plotting a cross-section through the dimer center along the X-axis. The valleys between two peaks represent the position of initial gold nanoparticles, which were canceled out during the image subtraction. As this figure indicates, the gap of the dimer is filled

dx.doi.org/10.1021/ph500331c | ACS Photonics 2015, 2, 121−129

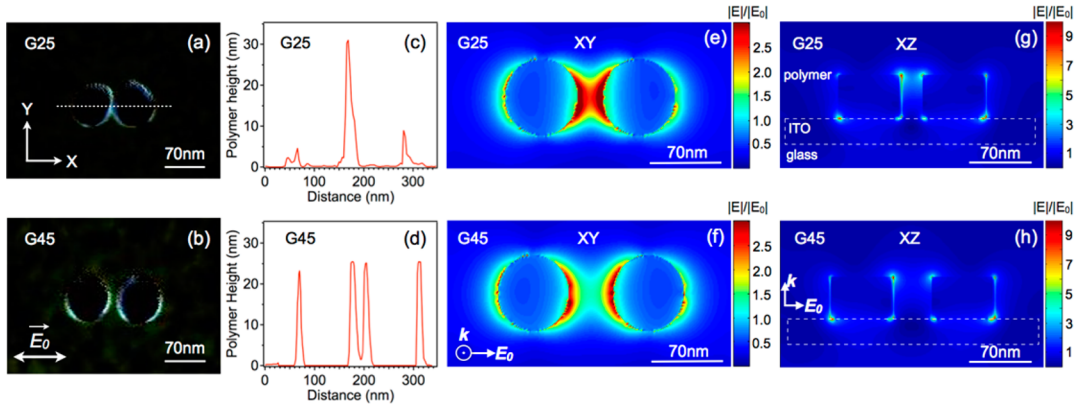

Figure 2. Profiles of two typical hybrid dimers with different initial gap sizes. Differential AFM images of hybrid dimers with (a) g = 25 nm and (b) g = 45 nm as initial gap sizes. Cross-section profiles of the differential AFM images along the *X*-axis for the two hybrid dimers (c) g = 25 nm and (d) g = 45 nm. (e and f) Top views of FDTD simulated normalized field distributions for initial gold dimers with 25 and 45 nm gap sizes, respectively. (g and h) Side views of FDTD simulated normalized field distributions for initial gold dimers with 25 and 45 nm gap sizes, respectively. The simulation was performed in a medium of $n = 1.48$ (refractive index of the solution before polymerization) and under illumination with a $\lambda_0 = 647$ nm incident plane wave that is linearly polarized along the *X*-axis as $\mathbf{E}_0$ indicates.

with photopolymer due to the plasmonic coupling between the two nanoparticles with a small separation (g = 25 nm). The plasmonic coupling causes field redistribution that confines most of the energy in the gap. This leads to a small polymer height at both ends of the long axis of the g = 25 nm dimer. In the case of a larger separation (g = 45 nm), two separate polymer nanostructures can be distinguished within the gap. The two gold nanodisks behave as two isolated nanoparticles due to weak plasmon coupling in the gap. A 3D-finite-difference time-domain (3D-FDTD) simulation on the electric field distributions confirmed our experimental observation. The simulation was performed with commercial software in a polymer (n = 1.48) with a 1 nm step size. The incident light was set at λ_0 = 647 nm and polarized along *X*-axis. Top views of simulated normalized electric field distribution on nanodimers for g = 25 and 45 nm are shown in Figure 2e and f, respectively. A strong gap field confinement can be observed within the gap of 25 nm. In comparison, the 45 nm gap presents much weaker plasmonic coupling. The field redistribution that occurs in the experiment as a function of decreasing gap size is in good agreement with the simulation. Side views of electric field (Figure 2g and 2h) further confirm the measured polymer distribution in panels c and d.

Plasmon Resonances of the Hybrid Nanodimers. To understand better the particle interactions within different gap sizes, hybrid nanodimers were characterized optically with dark-field scattering spectra (Figure 3). Each spectrum was collected on a single hybrid nanodimer with incident polarizations along either the long axis (Figure 3a) or the short axis (Figure 3b). The localized surface plasmon resonance (LSPR) of the short axis presents a constant peak at 625 nm. The long axis LSPR blue-shifts as the gap increases from 10 to 30 nm. It maintains a constant value at 628 nm as the gap increases from g = 30 to 50 nm. This suggests the vanishing of plasmon coupling between the two nanodisks of a hybrid particle pair starting from a spacing of 30 nm. The g = 0 nm dimer exhibits two plasmon modes. One of them is blue-shifted in LSPR compared to all other dimers due to a higher order plasmon mode. The spectra are in good agreement with the previously reported work on separated, touching, and overlapping particle pairs.[40−43] These studies illustrated red-shifted LSPRs as the particles approach before touching. Starting from a 0.5 nm gap,[43] a blue-shifted mode appears due to the transverse charge oscillation between the two

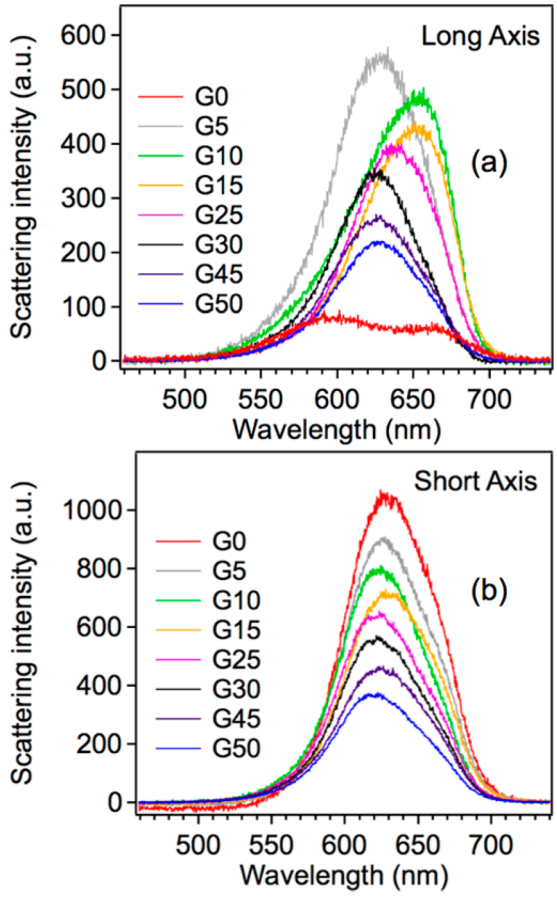

Figure 3. Scattering spectra of hybrid nanodimers with incident polarization along the (a) long axis and (b) short axis of the dimers. Each spectrum was collected from a unique hybrid nanodimer. Intensities have been set an offset to separate the spectra from one another.

nanodisks. As to the g = 5 nm dimer designed in our study, the longitudinal LSPR reads 628 nm, which suggests that the two particles are actually very slightly separated. Technologically, a 5 nm gap is rarely controllable by EBL due to the resolution of SEM. We could not obtain an image of this dimer showing a clear

dx.doi.org/10.1021/ph500331c | ACS Photonics 2015, 2, 121−129

gap because 5 nm is beyond the resolution of both the AFM and SEM.

Polarization-Dependent SERS Study on the Hybrid Dimers with Different Initial Particle Separations. By being trapped at the hotspot of the nanodimers via photopolymerization, MB molecules can be used for SERS study. The excitation wavelength λ_{exc} = 633 nm was adopted to take advantage of the absorption of methylene blue molecules. For each nanodimer, SERS signals were collected under two different incident polarizations along the *X* and *Y* axes, respectively. An acquisition time of 30 s and an incident power of 9.4 μW were applied for the collection of each spectrum. The size of the laser spot at the focal plane was about 1 μm. Figure 4 shows the SERS signals from a 10 nm gap nanodimer. As illustrated in the figure, we define

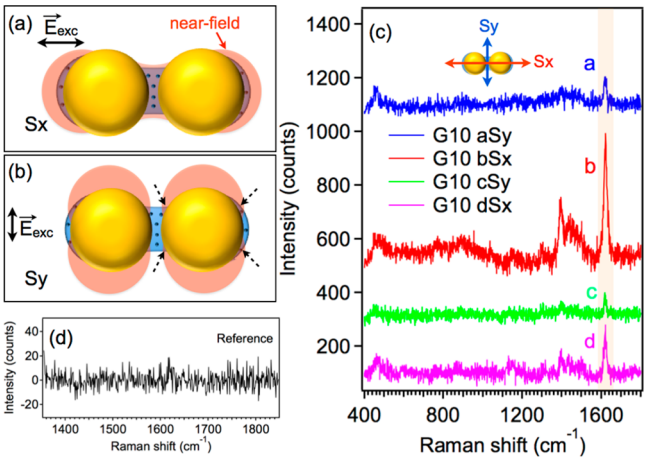

Figure 4. SERS spectra from a single hybrid nanodimer with a gap size of *g* = 10 nm. (a and b) Schemes of the two configurations for Sx and Sy, respectively, under different incident polarizations along the *X*-axis and the *Y*-axis. (c) Polarization-dependent Raman signals collected with an excitation wavelength of λ_{exc} = 633 nm in a chronological order of a−b−c−d as the legend shows. (d) Reference spectrum zoomed in the 1350−1850 cm^{-1} spectral region. The reference was collected 5 μm away from the nanostructure. Baselines have been subtracted. See Figure S1 for original spectra without any modification.

- Sx (Figure 4a) as the spectrum collected with an incident polarization along the long axis of the dimer. In this case, the near-field has a maximum spatial overlap with the MB distribution. All molecules trapped in the polymer nanostructure contributed to the SERS signal.
- Sy (Figure 4b) as the SERS spectrum collected with an incident polarization along the short axis of the dimer. In this situation, the spatial overlap between molecular distribution and near-field distribution is minimized. SERS signal comes mainly from a small number of trapped molecules that can be excited by the near-field under both polarizations (pointed out by dashed arrows on one nanodisk).

The SERS spectra were collected following a chronological order of a−b−c−d (Figure 4c). In other words, the spectrum with incident polarization perpendicular to the long axis was taken first (aSy), and then the one along the long axis (bSx) was collected. This procedure was repeated by cSy and dSx in order to confirm the result. The mode at $\Delta\bar{\nu}$ = 1620 cm^{-1}, which always displays a highest intensity, is used for further discussions. This mode corresponds to the stretching C−C ring of the MB molecule. The corresponding Raman wavelength λ_{Raman} = 705 nm can be deduced from the definition of Stokes shift $\Delta\bar{\nu} = (1/\lambda_{exc}) - (1/\lambda_{Raman})$. The reference spectrum (Figure 4d) that was collected from 5 μm away from the nanostructure does not reveal any Raman mode at 1620 cm^{-1}. More reference signals are presented in Figure S2, including the spectra from the polymer material without a metal nanoparticle, from a PETIA film without MB and from a glass substrate. All these reference spectra help to confirm that the 1620 cm^{-1} mode is from the MB molecules that are excited by the near-field of metal nanoparticles.

From Figure 4, three pieces of information can be obtained. First, for the spectra with the same incident polarizations, the intensity of the 1620 cm^{-1} mode decreases as time goes by (i.e., aSy > cSy, bSx > dSx). When the excitation wavelength matches the absorption of the dye (i.e., surface enhanced resonance Raman spectroscopy, SERRS), photobleaching occurs. The photobleaching, which is in essential reactions between molecules and environment (e.g., oxygen), finally leads to the detection of a non resonant SERS signal. This is exactly the situation in this study. Second, the intensity of the 1620 cm^{-1} mode of Sx decreases more rapidly than Sy. We can deduce a dSx/bSx = 0.4 and a cSy/aSy = 0.64 from the figure. The MB-doped photopolymer was integrated along the long axis (particularly in the gap) of the dimer. These molecules are excited primarily by the incident far-field when the polarization is along the short axis. In contrast, signals from molecules trapped in the polymer can be enhanced by the optical near-field with long-axis polarization. With this field enhancement, molecules are bleached more rapidly in the case of Sx due to higher local power. Third, Sx is always higher than Sy at the mode 1620 cm^{-1}. The baseline-corrected peak intensity of the *g* = 10 nm dimer increased by 4.6 times from 101 (aSy) to 460 counts (bSx) in the first cycle of collection (Figure 4c), and by 2.8 times from 65 (cSy) to 186 counts (dSx) in the second cycle (Figure 4d). It should be stressed that the scattering spectra (Figure 3) of this dimer indicate that the transverse mode LSPR is closer to the 633 nm excitation wavelength as compared to the longitudinal mode. The Sx > Sy effect is thus not due to a plasmon resonant effect. In order to avoid difficulties arising from photobleaching for interpreting Sx > Sy, we collected the SERS signal Sy before Sx. In the case of a highly symmetric nano-object, that is, a nanosphere with spatially isotropic dye distribution, it is reasonable to expect a lower intensity when the polarization is rotated by 90° from Sy to Sx due to photobleaching. For a dimer, Sx is able to overcome photobleaching and exceed Sy with considerable Raman intensity. This anisotropic Raman response (Sx > Sy) is the result of four factors. (1) Field confinement in the gap. (2) The spatial overlap of the near-field with the MB-doped polymer under longitudinal polarization of the excitation laser (i.e., the overlap effect illustrated in Figure 4a,b). (3) The plasmon resonance effect that has a greater contribution to Sy than to Sx at λ_{exc} = 633 nm (Figure 3, G10). The λ_{Raman} = 705 nm Raman field is out of the plasmon resonance of the dimers and is therefore believed to have no contribution to the resonance effect. (4) Photobleaching that highly depends on the LSPR of the metal nanoparticle. It is worth noticing that the gap effect and the spatial overlap effect help enhancing Sx, while the plasmon resonance and photobleaching effects tend to produce a weaker Sx compared to Sy.

The effect we would like to highlight in this part is the spatial overlap (item 2 above) effect. This effect is specific to the anisotropic hybrid structure. In order to highlight the significance of molecular trapping at plasmonic hotspots, we carried out three

dx.doi.org/10.1021/ph500331c | ACS Photonics 2015, 2, 121−129

additional studies. The first one is polarization-dependent SERS study on the hybrid dimers (dye molecules positioned mainly at plasmonic hotspots) with different initial particle separations. The other two are control experiments: polarization-dependent SERS studies on gold nanodimers with MB molecules randomly distributed and on an isolated hybrid nanodisk. For the hybrid nanodimers with MB molecules selectively positioned, the baseline-corrected intensities at 1620 cm^{-1} are plotted in Figure 5a for Sy (blue dot) and Sx (red square) as a function of gap size.

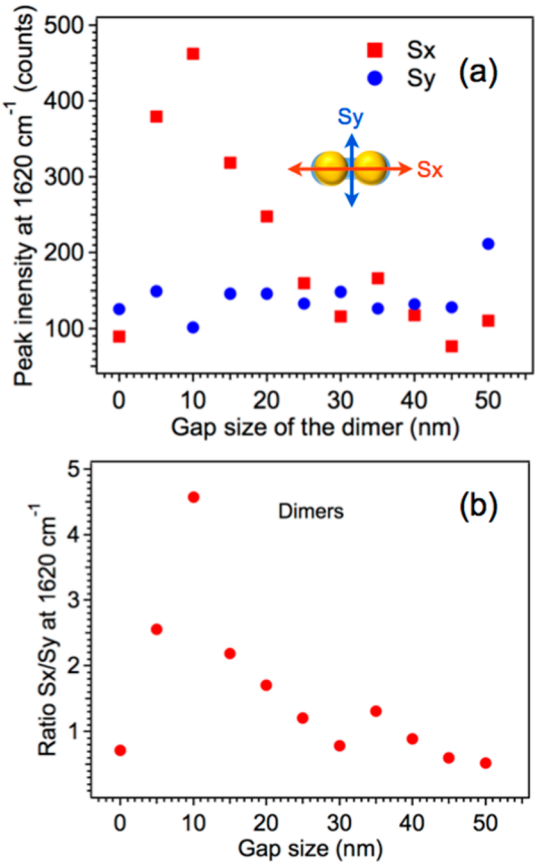

Figure 5. (a) Baseline-corrected Raman intensity at 1620 cm^{-1} for both Sy (blue dot) and Sx (red square). (b) Ratio of Sx/Sy of the 1620 cm^{-1} mode on dimers showing the anisotropy of SERS signal.

Sy presents a flat Raman intensity as a function of gap distance, whereas Sx varies as the gap increases. In the case of $g = 0$, when no gap exists (and therefore no molecule) between the two nanodisks, Sx is at the same level as Sy. The signal is at its maximum value when the gap size is equal to 10 nm. Beyond 10 nm and as the gap keeps increasing, Sx decreases progressively to the same level of intensity as Sy at $g = 30$ nm. The different trends of Sy and Sx result from the anisotropic geometry of the hybrid nanostructure, involving the electromagnetic enhancement of gold nanodimers, the anisotropic spatial distribution of MB, as well as the efficiency of photopolymerization that determines the volume of integrated polymer and the number of MB molecules trapped. For some of the dimers, particularly those with larger gaps ($g = 30$ nm to $g = 50$ nm), Sx fluctuates at the same level as Sy. In the case of these large gaps, the field confinement in the gap does not exist. This fluctuation is due to the competition between the signal enhancements caused by MB-doped polymer along the long axis and the photobleaching of MB molecules after the acquisition of Sy. It should be highlighted that the longitudinal mode LSPRs of these large gap dimers are closer to the excitation wavelength $\lambda_{exc} = 633$ nm as compared to the strongly coupled nanodimers (see Figure 3). The plasmon resonance thus helps accelerate the photobleaching of dye molecules in the hybrid dimers with large initial gaps, leading to a balance between the photobleaching and the overlap effect. The maximum SERS enhancement of Sx at $g = 10$ nm is therefore a result of both field confinement in the gap and the overlap effect, instead of the on-resonance plasmon excitation of the nanostructure.

To confirm the result, FDTD simulations were performed for the SERS gain from mode 1620 cm^{-1} under an incident polarization along the X and *Y*-axes. Figure 6a shows the

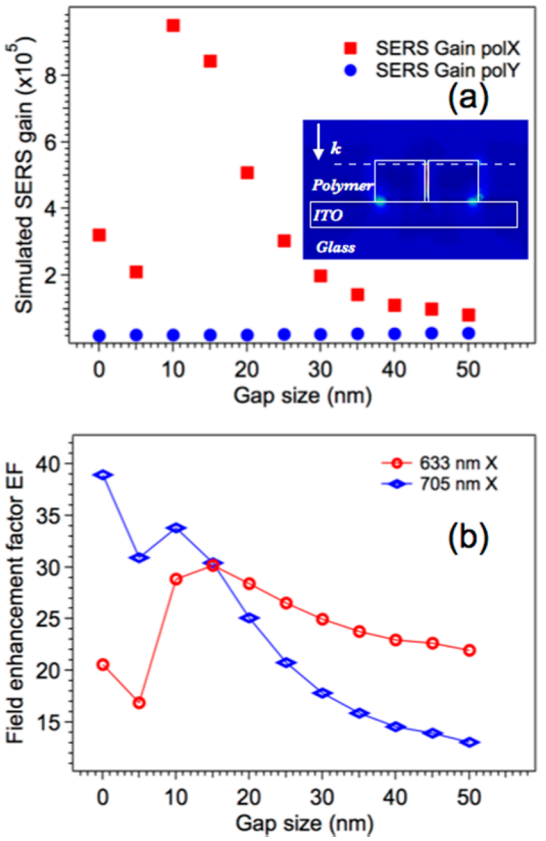

Figure 6. (a) FDTD simulated maximum SERS gain under *X* (red square) and *Y* (blue dot) polarizations in the XY plane that is 45 nm above the ITO layer (dashed line shown in the inset). (b) Simulated field enhancement factor for the incident field $\lambda_{exc} = 633$ nm (red circle) and the Raman field $\lambda_{Raman} = 705$ nm (blue rhomb) under *X*-polarization. The models applied for the simulations were gold nanodimers placed on ITO coated glass substrate in a photopolymer ($n = 1.48$).

maximum SERS gain in the *XY* plane that is placed 45 nm above the ITO layer (dashed line in the inset). The simulation was carried out based on the approximation[44,45]

$$G_{SERS} \propto \left|\frac{E_{loc}(\lambda_{exc})}{E_{inc}(\lambda_{exc})}\right|^2 \left|\frac{E_{result}(\lambda_{Raman})}{E_{rad}(\lambda_{Raman})}\right|^2 = g(\lambda_{exc})g(\lambda_{Raman}) \quad (1)$$

where $g(\lambda_{exc})$ and $g(\lambda_{Raman})$ are the enhancement factor for the incident field intensity and the Raman field intensity, respectively. The first factor $g(\lambda_{exc}) = |E_{loc}(\lambda_{exc})/E_{inc}(\lambda_{exc})|^2$ in eq 1 results from the modification of the excitation field caused

dx.doi.org/10.1021/ph500331c | ACS Photonics 2015, 2, 121−129

by the nanoparticle. The second factor $g(\lambda_{Raman}) = |E_{result}(\lambda_{Raman})/E_{rad}(\lambda_{Raman})|^2$ describes the enhancement of the radiative field caused by the nanoparticle. The molecular dipole behaves as the source of the radiative field in the latter situation. The enhancement factors of the excitation field $E_{loc}(\lambda_{exc})/E_{inc}(\lambda_{exc})$ and the Raman field $E_{result}(\lambda_{Raman})/E_{rad}(\lambda_{Raman})$ polarized along *X*-axis are plotted in Figure 6b as red circles and blue rhombs, respectively. The model for FDTD simulation used isotropic surrounding medium. Despite this point, Figure 6 is highly relevant to our AHN instead of classical SERS because the field redistribution in the gap volume of strongly coupled nanodimers has an indispensable contribution to the SERS gain. In classical SERS (refer to control experiment I below), molecules appear only on the nanoparticle surface and the volume in the gap does not contribute to the SERS effect because of the absence of probe molecules. In comparison, our hybrid nanostructures position molecules within this volume to take part in SERS. The FDTD simulation considers each point in the space to contain SERS probe molecules and plot maximum SERS gain in Figure 6. The simulated SERS gain presents a similar trend to the experiment but polarization sensitivity reads higher. This is mainly due to the fact that the simulation gives a maximum value in the detection plane (dashed line in the inset of Figure 6a), while the experiment measures a sum value in the entire detection region (1 μm diameter in the *XY* plane). The simulated SERS gain reaches a maximum at the 10 nm gap, which is in good agreement with the experiment. At smaller gap sizes, the Raman field tends to contribute more than the excitation field because the plasmon resonances of these dimers are closer to the Raman field wavelength λ_{Raman} = 705 nm as compared to larger gap sizes. The situation inverts for the larger gap sizes.

Control Experiment I: Random Molecule Distribution around Nanodimers. To analyze the contribution of anisotropy introduced by photopolymerization, a control experiment was performed on gold nanodimers that are covered with a layer of MB molecules. MB molecules dissolved in ethanol were spin-coated on the gold nanodimers. Rinsing with ethanol followed in order to remove the unattached molecules. In this way, MB molecules can be considered to be randomly distributed around the nanoparticles. SERS signals were detected in the same way as for the hybrid systems. Baseline-corrected Raman intensity at 1620 cm^{-1} for Sy (blue circle) and Sx (red square) are plotted in Figure 7a. Unlike the hybrid nanostructures, these nanodimers do not present a polarization-dependent SERS response except for contacted particles ($g = 0$). Other than a very obvious polarization-dependent Sx/Sy at $g = 0$, the ratio at other gap sizes fluctuates near 1, showing no polarization dependence (Figure 7b). Previous studies on the gap-modified SERS have shown as well that a small gap size (<5 nm) is usually required when obvious polarization dependence is expected.[17,46,47] Note that, in this control experiment, molecules are more likely to be attached on the particle surface. For the touching dimer, SERS intensity along the long axis is obviously higher than the short axis because of the singular response at the contact crevice.[48,49] The difference between Figure 5 and Figure 7 confirms the trapping of MB molecules at plasmonic hotspots and their contribution to the optical anisotropy.

Control Experiment II: Anisotropic Hybrid Nanodisk. The AHNs can be constructed not only on the basis of coupled nanoparticles, but also on simple metal nanostructures. We take a monomer of gold nanodisk as an example to confirm this point. MB molecules were placed along the *X*-axis of a gold nanodisk (R = 90 nm in radius and h = 50 nm in height) by the photopolymer

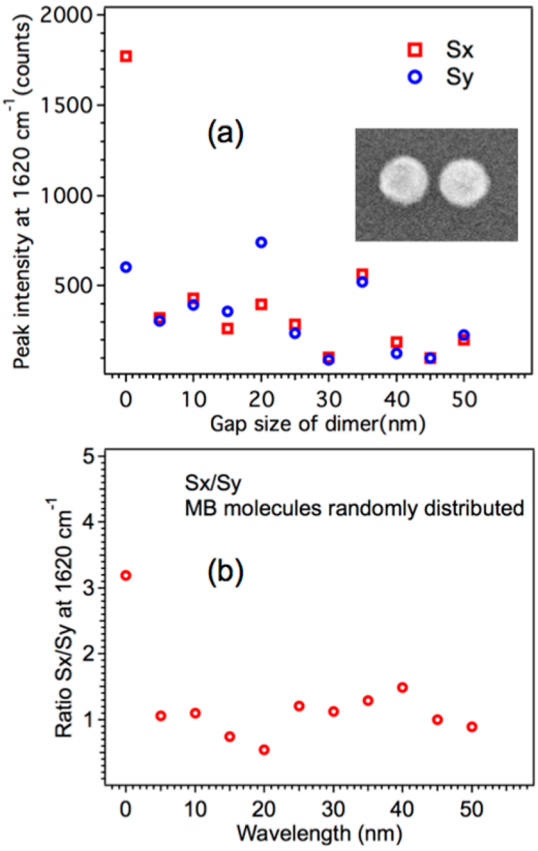

Figure 7. Control experiment with MB randomly distributed around the nanoparticles (a) Baseline-corrected Raman intensity at 1620 cm^{-1} for both Sy (blue circle) and Sx (red square). (b) The ratio of Sx/Sy for the 1620 cm^{-1} mode on dimers showing the anisotropy of SERS signal.

nanostructures integrated with the dipolar off-resonance surface plasmons. This nanodisk has a LSPR in the near-infrared range[50] and is therefore in the off-resonance case for both photopolymerization (λ_0 = 647 nm) and SERS (λ_{exc} = 633 nm). The Raman signals Sy (in blue) and Sx (in red) were collected with an incident polarization perpendicular and parallel to the photopolymer, respectively (Figure 8a). Sx was collected after Sy, repeating the procedures for dimers. One can still recognize a higher Sx than Sy at 1620 cm^{-1}. The collection of SERS signals Sy and Sx was repeated three times on this isolated hybrid nanodisk. As Figure 8b demonstrates, the Raman intensity at 1620 cm^{-1} presents reproducible polarization-dependence: Sx > Sy.

Compared to the dimers with large gaps (R = 35 nm, $g \geq 30$ nm, LSPR at 625 nm), the LSPR of the isolated nanodisk is much farther from the excitation wavelength λ_{exc} = 633 nm. The off-resonance excitation on the isolated hybrid nanodisk makes the photobleaching of MB molecules slower in comparison with the hybrid nanodimer. As a result, Sx from MB molecules in the isolated hybrid nanodisk is strong enough to balance the photobleaching during the acquisition of Sy and exceeds Sy by a factor of 1.48.

In conclusion, this article presents a self-developed anisotropic hybrid nanosystem for dye molecule positioning at plasmonic hotspots. It was further utilized for a SERS study to reveal the significance of trapped molecules that do not adsorb on a particle surface. The AHN is constructed by nanophotopolymerization triggered by the plasmonic field supported by metal nanostructures. Using dimers and monomers of gold nanodisks, dye molecules can be trapped successfully in the photopolymer

dx.doi.org/10.1021/ph500331c | *ACS Photonics* 2015, 2, 121−129

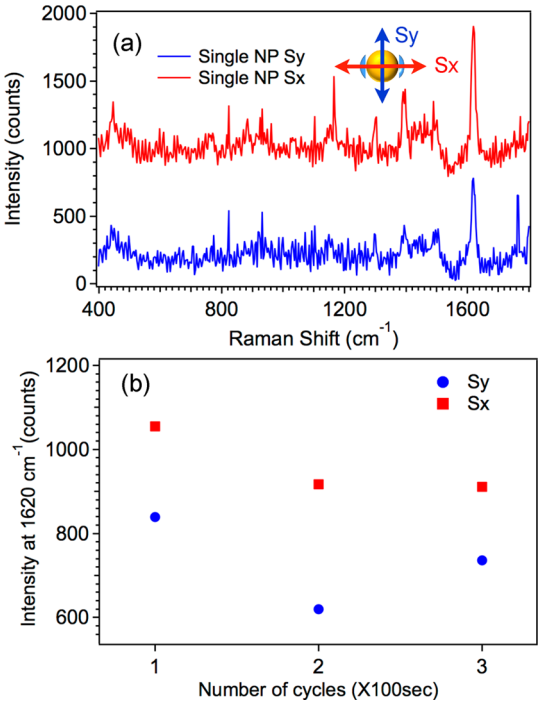

Figure 8. (a) SERS signals from a single hybrid system of isolated gold nanodisk/MB-doped photopolymer. (b) Raman intensities at 1620 cm $^{-1}$ for both Sy (blue dot) and Sx (red square) on the hybrid nanostructure.

nanostructures, whose optical distribution is highly controllable with the incident polarization during polymerization. With MB molecules trapped mainly in the gap, SERS intensity from the hybrid nanodimer was highly related to the gap size and the polarization of excitation light. In particular, the effect of the anisotropic distribution of the active medium has been demonstrated and discussed in terms of spatial overlap between the plasmonic near field and the dye-containing polymer. Further study carried out on isolated gold nanodisk indicates that such an AHN is achievable not only on coupled particle pairs, but also on simple nanostructures. This article used SERS as an example for one of the numerous potential applications of our AHN where the spatial distribution of the active medium is controllable. In the photopolymerizable formulation, MB can be substituted by other fluorophores for surface-enhanced spectroscopic studies. For further uses of this nanohybrid, other types of functional materials such as quantum dots, conductive molecules, or biomolecules can be doped as well in the polymer nanostructures.

■ ASSOCIATED CONTENT

Supporting Information

We provide an additional file, including the reference Raman spectra, original SERS spectra on G10 hybrid dimer, and a system stability test as complementary data. This material is available free of charge via the Internet at http://pubs.acs.org.

■ AUTHOR INFORMATION

Corresponding Author

*E-mail: renaud.bachelot@utt.fr.

Present Addresses

[‡]Department of Chemistry, University of Illinois at Urbana−Champaign, 600 South Mathews Avenue, Roger Adams Laboratory 60, Box 100−5, Urbana, Illinois 61801, U.S.A. (X.Z.).
[§]Laboratoire de Photonique et de Nanostructures LPN - CNRS, Route de Nozay, 91460 Marcoussis, France (C.D.).
[¶]State Key Laboratory of Low-Dimensional Quantum Physics, Department of Physics, Tsinghua University, Beijing 100084, China (H.W.).

Notes

The authors declare no competing financial interest.

■ ACKNOWLEDGMENTS

The authors would like to thank the platform Nano'mat, the HAPPLE Project (ANR-12-BS10-0016) funded by Agence Nationale de la Recherche (ANR), as well as the Partner University Fund (PUF) Project. Use of the Center for Nanoscale Materials was supported by the U.S. Department of Energy, Office of Science, Office of Basic Energy Sciences, under Contract No. DE-AC02-06CH11357. This work has been carried out in the general context of the Labex ACTION.

■ REFERENCES

(1) Kinkhabwala, A.; Yu, Z.; Fan, S.; Avlasevich, Y.; Müllen, K.; Moerner, W. E. Large Single-Molecule Fluorescence Enhancements Produced by a Bowtie Nanoantenna. *Nat. Photonics* **2009**, *3*, 654−657.

(2) Ming, T.; Zhao, L.; Yang, Z.; Chen, H.; Sun, L.; Wang, J.; Yan, C. Strong Polarization Dependence of Plasmon-Enhanced Fluorescence on Single Gold Nanorods. *Nano Lett.* **2009**, *9*, 3896−3903.

(3) Dulkeith, E.; Morteani, A. C.; Niedereichholz, T.; Klar, T. A.; Feldmann, J. Fluorescence Quenching of Dye Molecules near Gold Nanoparticles: Radiative and Nonradiative Effects. *Phys. Rev. Lett.* **2002**, *89*, 203002.

(4) Noginov, M. A.; Zhu, G.; Belgrave, A. M.; Bakker, R.; Shalaev, V. M.; Narimanov, E. E.; Stout, S.; Herz, E.; Suteewong, T.; Wiesner, U. Demonstration of a Spaser-Based Nanolaser. *Nature* **2009**, *460*, 1110−1112.

(5) Zhao, L.; Ming, T.; Shao, L.; Chen, H.; Wang, J. Plasmon-Controlled Forster Resonance Energy Transfer. *J. Phys. Chem. C* **2012**, *116*, 8287−8296.

(6) Brown, M. D.; Suteewong, T.; Kumar, R. S.; D'Innocenzo, V.; Petrozza, A.; Lee, M. M.; Wiesner, U.; Snaith, H. J. Plasmonic Dye-Sensitized Solar Cells Using Core-Shell Metal-Insulator Nanoparticles. *Nano Lett.* **2011**, *11*, 438−455.

(7) Standridge, S. D.; Schatz, G. C.; Hupp, J. T. Distance Dependence of Plasmon-Enhanced Photocurrent in Dye-Sensitized Solar Cells. *J. Am. Chem. Soc.* **2009**, *131*, 8407−8409.

(8) Mayer, K. M.; Lee, S.; Liao, H.; Rostro, B. C.; Fuentes, A.; Scully, P. T.; Nehl, C. L.; Hafner, J. H. A Lable-Free Immunoassay Based Upon Localized Surface Plasmon Resonance of Gold Nanorods. *ACS Nano* **2008**, *2*, 687−692.

(9) Li, Z.-Y.; Xia, Y. Metal Nanoparticles with Gain toward Single-Molecule Detection by Surface-Enhanced Raman Scattering. *Nano Lett.* **2010**, *10*, 243−249.

(10) Hoppener, C.; Novotny, L. Antenna-Based Optical Imaging of Single Ca^{2+} Transmembrane Proteins in Liquids. *Nano Lett.* **2008**, *8*, 642−646.

(11) Le Ru, E. C.; Grand, J.; Sow, I.; Somerville, W. R. C.; Etchegoin, P. G.; Treguer-Delapierre, M.; Charron, G.; Félidj, N.; Lévi, G.; Aubard, J. A Scheme for Detecting Every Single Target Molecule with Surface-Enhanced Raman Spectroscopy. *Nano Lett.* **2011**, *11*, 5013−5019.

(12) Wang, L.; Liu, Y.; Li, W.; Jiang, X.; Ji, Y.; Wu, X.; Xu, L.; Qiu, Y.; Zhao, K.; Wei, T.; Li, Y.; Zhao, Y.; Chen, C. Selective Targeting of Gold Nanorods at the Mitochondria of Cancer Cells: Implications for Cancer Therapy. *Nano Lett.* **2011**, *11*, 772−780.

(13) Gobin, A. M.; Lee, M. H.; Halas, N. J.; James, W. D.; Drezek, R. A.; West, J. L. Near-Infrared Resonant Nanoshells for Combined Optical Imaging and Photothermal Cancer Therapy. *Nano Lett.* **2007**, *7*, 1929−1934.
(14) Cortés, E.; Etchegoin, P. G.; Le Ru, E. C.; Fainstein, A.; Vela, M. E.; Salvarezza, R. C. Monitoring the Electrochemistry of Single Molecules by Surface-Enhanced Raman Spectroscopy. *J. Am. Chem. Soc.* **2010**, *132*, 18034−18037.
(15) Xu, J.-Y.; Chen, T.-W.; Bao, W.-J.; Wang, K.; Xia, X.-H. Label-Free Strategy for In-Situ Analysis of Protein Binding Interaction Based on Attenuated Total Reflection Surface Enhanced Infrared Absorption Spectroscopy (ATR-SEIRAS). *Langmuir* **2012**, *28*, 17564−17570.
(16) McLellan, J. M.; Li, Z.-Y.; Siekkinen, A. R.; Xia, Y. The SERS Activity of Supported Ag Nanocubes Strongly Depends on Its Orientation Relative to Laser Polarization. *Nano Lett.* **2007**, *7*, 1013−1017.
(17) Ward, D. R.; Grady, N. K.; Levin, C. S.; Halas, N. J.; Wu, Y.; Nordlander, P.; Natelson, D. Electromigrated Nanoscale Gaps for Surface-Enhanced Raman Spectroscopy. *Nano Lett.* **2007**, *7*, 1396−1400.
(18) Nath, N.; Chikoti, A. Label-Free Biosensing by Surface Plasmon Resonance of Nanoparticles on Glass: Optimization of Nanoparticle Size. *Anal. Chem.* **2004**, *76*, 5370−5378.
(19) Papadopoulou, E.; Bell, S. E. J. Surface-Enhanced Raman Evidence of Protonation Reorientation and Ag+ Complexation of Deoxyadenosine and Deoxyadenosine-5′-monophosphate (dAMP) on Ag and Au Surfaces. *J. Phys. Chem. C* **2011**, *115*, 14228−14235.
(20) Reineck, P.; Gomez, D.; Ng, S. H.; Karg, M.; Bell, T.; Mulvaney, P.; Bach, U. Distance and Wavelength Dependent Quenching of Molecular Fluorescence by Au@SiO_2 Core-Shell Nanoparticles. *ACS Nano* **2013**, *7*, 6636−6648.
(21) Ameer, F. S.; Hu, W.; Ansar, S. M.; Siriwardana, K.; Collier, W. E.; Zou, S.; Zhang, D. Robust and Reproducible Quantification of SERS Enhancement Factors Using a Combination of Time-Resolved Raman Spectroscopy and Solvent Internal Reference Method. *J. Phys. Chem. C* **2013**, *117*, 3483−3488.
(22) Song, J.; Zhou, J.; Duan, H. Self-Assembled Plasmon Vesicles of SERS-Encoded Amphiphilic Gold Nanoparticles for Cancer Cell Targeting and Traceable Intracellular Drug Delivery. *J. Am. Chem. Soc.* **2012**, *134*, 13458−13469.
(23) Kotnala, A.; Gordon, R. Quantification of High-Efficiency Trapping of Nanoparticles in a Double Nanohole Optical Tweezer. *Nano Lett.* **2014**, *14*, 853−856.
(24) Grigorenko, A. N.; Roberts, N. W.; Dickinson, M. R.; Zhang, Y. Nanometric Optical Tweezers Based on Nanostructured Substrates. *Nat. Photonics* **2008**, *2*, 365−370.
(25) Righini, M.; Zelenina, A. S.; Girard, C.; Quidant, R. Parallel and Selective Trapping in a Patterned Plasmonic Landscape. *Nat. Phys.* **2007**, *3*, 477−480.
(26) Fan, J. A.; He, Y.; Bao, K.; Wu, C.; Bao, J.; Schade, N. B.; Manoharan, V. N.; Shvets, G.; Nordlander, P.; Liu, D. R.; Capasso, F. DNA-Enabled Self-Assembly of Plasmonic Nanoscusters. *Nano Lett.* **2011**, *11*, 4859−4864.
(27) Gandra, N.; Abbas, A.; Tian, L.; Singamaneni, S. Plasmonic Planet-Satellite Analogues: Hierarchical Self-Assembly of Gold Nanostructures. *Nano Lett.* **2012**, *12*, 2645−2651.
(28) Galloway, C. M.; Kreuzer, M. P.; Acimovic, S. S.; Volpe, G.; Correia, M.; Petersen, S. B.; Neves-Petersen, M. T.; Quidant, R. Plasmon-Assisted Delivery of Single Nano-Objects in an Optical Hot Spot. *Nano Lett.* **2013**, *13*, 4299−4304.
(29) Wark, A. W.; Stokes, R. J.; Darby, S. B.; Smith, W. E.; Graham, D. Dynamic Imaging Analysis of SERS-Active Nanoparticle Clusters in Suspension. *J. Phys. Chem. C* **2010**, *114*, 18115−18120.
(30) Tay, L.-L.; Hulse, J.; Kennedy, D.; Pezacki, J. P. Surface-Enhanced Raman and Resonant Rayleigh Scatterings from Adsorbate Saturated Nanoparticles. *J. Phys. Chem. C* **2010**, *114*, 7356−7363.
(31) Rycenga, M.; Camargo, P. H. C.; Li, W.; Moran, C. H.; Xia, Y. Understanding the SERS Effects of Single Silver Nanoparticles and Their Dimers, One at a Time. *J. Phys. Chem. Lett.* **2010**, 696−703.
(32) McLellan, J. M.; Li, Z.-Y.; Siekkinen, A. R.; Xia, Y. The SERS Activity of Supported Ag Nanocubes Strongly Depends on Its Orientation Relative to Laser Polarization. *Nano Lett.* **2007**, *7*, 1013−1017.
(33) Ibn El Ahrach, H.; Bachelot, R.; Vial, A.; Lérondel, G.; Plain, J.; Royer, P.; Soppera, O. Spectral Degeneracy Breaking of the Plasmon Resonance of Single Metal Nanoparticles by Nanoscale Near-Field Photopolymerization. *Phys. Rev. Lett.* **2007**, *98*, 107402.
(34) Deeb, C.; Bachelot, R.; Plain, J.; Baudrion, A.-L.; Jradi, S.; Bouhelier, A.; Soppera, O.; Jain, P. K.; Huang, L.; Ecoffet, C.; Balan, L.; Royer, P. Quantitative Analysis of Localized Surface Plasmons based on Molecular Probing. *ACS Nano* **2010**, *4*, 4579−4586.
(35) Espanet, A.; Dos Santos, G.; Ecoffet, C.; Lougnot, D. J. Photopolymerization by Evanescent Waves: Characterization of Photopolymerizable Formulation for Photolithography with Numeric Resolution. *Appl. Surf. Sci.* **1999**, *138−139*, 87−92.
(36) Deeb, C.; Ecoffet, C.; Bachelot, R.; Plain, J.; Bouhelier, A.; Soppera, O. Plasmon-Based Free-Rdical Photopolymerization: Effect of Diffusion on Nanolithography Process. *J. Am. Chem. Soc.* **2011**, *133*, 10535−10542.
(37) Deeb, C.; Zhou, X.; Plain, J.; Wiederrecht, G.; Bachelot, R.; Russell, M.; Jain, P. K. Size Dependence of Plasmonic Near-Field Measured via Single Nanoparticle Photoimaging. *J. Phys. Chem. C* **2013**, *117*, 10669−10676.
(38) Deeb, C.; Zhou, X.; Miller, R.; Gray, S. K.; Marguet, S.; Plain, J.; Wiederrecht, G. P.; Bachelot, R. Mapping the Electromagnetic Near-Field Enhancements of Gold Nanocubes. *J. Phys. Chem. C* **2012**, *116*, 24734−24740.
(39) Deeb, C.; Zhou, X.; Gérard, D.; Bouhelier, A.; Jain, P. K.; Plain, J.; Soppera, O.; Royer, P.; Bachelot, R. Off-Resonant Optical Excitation of Gold Nanorods: Nanoscale Imprint of Polarization Surface Charge Distribution. *J. Phys. Chem. Lett.* **2011**, *2*, 7−11.
(40) Atay, T.; Song, J.-H.; Nurmikko, A. V. Strongly Interacting Plasmon Nanoparticle Paris: from Dipole-Dipole Interaction to Conductively Coupled Regime. *Nano Lett.* **2004**, *4*, 1627−1631.
(41) McMahon, J. M.; Henry, A.-I.; Wustholz, K. L.; Natan, M. J.; Freeman, R. G.; Van Duyne, R. P.; Schatz, G. C. Gold Nanoparticle Dimer Plasmonic: Finite Element Method Calculations of the Electromagnetic Enhancement to Surface-Enhanced Raman Spectroscopy. *Anal. Bioanal. Chem.* **2009**, *394*, 1819−1825.
(42) Lassiter, J. B.; Aizpurua, J.; Hernandez, L. I.; Brandl, D. W.; Romero, I.; Lal, S.; Hafner, J. H.; Nordlander, P.; Halas, N. J. Close Encounters Between Two Nanoshells. *Nano Lett.* **2008**, *8*, 1212−1218.
(43) Zuloaga, J.; Prodan, E.; Nordlander, P. Quantum Description of the Plasmon Resonances of a Nanoparticle Dimer. *Nano Lett.* **2009**, *9*, 887−891.
(44) Félidj, N.; Aubard, J.; Lévi, G.; Kreen, J. R.; Salerno, M.; Schider, G.; Lamprecht, B.; Leitner, A.; Aussenegg, R. Controlling the Optical Response of Regular Arrays of Gold Particles for Surface-Enhanced Raman Scattering. *Phys. Rev. B* **2002**, *65*, 075419.
(45) Grimault, A.-S.; Vial, A.; Lamy de la Chapelle, M. Modeling of Regular Gold Nanostructures Arrays for SERS Applications Using a 3D FDTD Method. *Appl. Phys. B: Laser Opt.* **2006**, *84*, 111−115.
(46) Rycenga, M.; Camargo, P. H. C.; Li, W.; Moran, C. H.; Xia, Y. Understanding the SERS Effects of Single Silver Nanoparticles and Their Dimers, One at a Time. *J. Phys. Chem. Lett.* **2010**, *1*, 696−703.
(47) Talley, C. E.; Jackson, J. B.; Oubre, C.; Grady, N. K.; Hollars, C. W.; Lane, S. M.; Huser, T. R.; Nordlander, P.; Halas, N. J. Surface-Enhanced Raman Scattering from Individual Au Nanoparticles and Nanoparticle Dimer Substrates. *Nano Lett.* **2005**, *5*, 1569−1574.
(48) Savage, K. J.; Hawkeye, M. M.; Esteban, R.; Borisov, A. G.; Aizpurua, J.; Baumberg, J. J. Revealing the Quantum Regime in Tunneling Plasmonics. *Nature* **2012**, *491*, 574−577.
(49) Romero, I.; Aizpurua, J.; Bryant, G. W.; Javier Garcia de Abajo, F. Plasmons in Nearly Touching Metallic Nanoparticles: Singular Response in the Limit of Touching Dimers. *Opt. Exp.* **2006**, *14*, 9988−9999.

(50) Viste, P.; Plain, J.; Jaffiol, R.; Vial, A.; Adam, P. M.; Royer, P. Enhancement and Quenching Regimes in Metal-Semiconductor Hybrid Optical Nanosources. *ACS Nano* **2010**, *4*, 759−764.